JOURNAL OF AIRCRAFT
Vol. 36, No. 3, May–June 1999

Directional Stability and Control During Landing Rollout

Malcolm J. Abzug*
Pacific Palisades, California 90272-4428

Directional stability in landing rollout of the tricycle landing gear arrangement used in light airplanes is shown in a computer replication of a 1935 demonstration. Stability derivatives of aircraft tires are developed based on rolling tire experimental data. A small perturbation analysis using the tire stability derivatives provides a simplified model of the rollout problem, for better understanding and for checks on complete simulations. Eigenvalues in rollout are found for three cases, a sailplane, a light plane, and a large jet transport. A nonlinear transient analysis is used to verify the small perturbation model, for the sailplane case. Castering wheels are found to make negligible contributions to the eigenvalues. The position of the main gear with respect to the c.g. dominates the problem, aft gears being stable. Large airplanes with noncastering nose wheels appear to be stable in rollout over their ranges of airspeed and relative main gear to nose gear loadings. In transient analysis, banking into the swerve, a nonintuitive strategy for avoiding running off runways in side winds, is shown to be effective for bicycle gears, and in particular, for advanced sailplanes with main wheels ahead of the c.g.

Nomenclature

b_w = aircraft wingspan
C_L = lift coefficient
C_{nr}, C_{yr} = aircraft yawing derivatives (no tires)
$C_{n\beta}$, $C_{y\beta}$ = aircraft sideslip derivatives (no tires)
F_x, F_y, F_z = forces applied by the ground to the tires: traction, lateral, and vertical
I_z = aircraft moment of inertia in yaw
LY, SQ, τ = intermediate dimensional variables
M_z = tire self-aligning torque
m = aircraft mass
N = aircraft yawing moment
N_r, Y_r = dimensional yawing derivatives
N_v, Y_v = dimensional sideslip derivatives
n_α = derivative of M_z/F_z with slip angle
PS = tire steering angle
R, r = yawing velocity, perturbation R
S = tire longitudinal slip ratio, ratio of forward speed less tire peripheral speed, divided by the forward speed
S_w = aircraft wing area
U, V = aircraft velocity components along X and Y body axes
u, v = tire longitudinal and lateral velocities relative to the ground
XN, YN, ZN = tire contact point locations relative to aircraft X, Y, and Z body axes
y_α = derivative of F_y/F_z with slip angle
y_γ = derivative of F_y/F_z with camber angle
ZLG(K) = Z-body force applied by landing gear to airframe, positive downward, K is the tire index number, see Fig. 4
α = angle of attack, or lateral slip angle, depending on context
β = sideslip angle
γ = camber angle, or tire bank angle
Δ = increment as a result of tire forces
ζ = castering damping ratio
θ = pitch attitude angle
μ = normalized traction force, $-F_x/F_z$
φ = perturbation bank angle
ω = castering natural frequency

Subscript

0 = reference steady-state condition

Received Aug. 3, 1998; revision received Oct. 21, 1998; accepted for publication Nov. 23, 1998.

*Aeronautical Consultant, 14951 Camarosa Drive. AIAA Fellow.

Introduction

THE modern light plane tricycle landing gear has main wheels behind the c.g. and a castering nose wheel ahead of the c.g. That arrangement put an end to the ground loop, which had been a problem with tail wheel landing gears. The ground loop is a loss in directional stability during ground rolls, which if uncorrected, causes a rapid yaw from the runway heading and a swerve off the runway.

The first castering nose wheel was most likely used on Weick's W-1 pusher of 1934.[1] Weick reported that castering the nose wheel improved directional stability in ground rolls. Weick demonstrated the directional stability advantage of the tricycle landing gear the following year, during an NACA aircraft engineering research conference at Langley Field, Virginia. He built framework models of both tail wheel and tricycle landing gear arrangements, and launched them down a ramp onto a concrete floor. The tail wheel model ground looped every time. The tricycle model ran straight, even when launched at yaw angle to the direction of motion.

Neither drawings of Weick's models nor movies of the demonstration have been located at the NASA Langley Research Center. However, modern pneumatic tire force and moment data, and computer simulation technology have made it possible to replicate the Weick 1935 demonstration. This same data and technology are used to revisit the rollout directional stability subject, to put it on a firmer basis than previous qualitative explanations.[2]

Assumptions and Limitations of the Analysis

The landing rollout directional stability and control problem starts when the aircraft's landing gear first touches the ground and continues down to low taxi speeds. Aerodynamic forces dominate at first, then tire forces dominate the rollout. A complete six-degrees-of-freedom analysis, which adds the dynamics of the wheels and struts to the aircraft equations of motion, is usually needed to deal adequately with this very complex problem.

Yet, it is good engineering practice when faced with complex nonlinear problems to derive as many simplified system models as possible, both for better understanding and for a check on segments of the complete analysis. The underlying assumptions of the

simplified models must be understood, to avoid misleading rather than helping the design engineer.

The well-known principles of small perturbation analysis are applied here to derive a class of simplified models for the landing rollout directional stability and control problem. In addition to the small-perturbation assumption, the following simplifications are made:

1) The bank angle is controlled to zero, reducing the lateral perturbation degrees of freedom to just sideslip and yawing velocity.

2) Wheel and strut masses are lumped with the rest of the airframe. That is, wheel and strut dynamics with respect to the airframe are neglected.

3) Multiple tires in a bogie are lumped as an equivalent single tire.

Braking and nonzero tire slip ratios can be accommodated within the analysis by choice of parameters.

The small perturbation analysis is thought to apply well at all rollout speeds to sailplanes, which usually have unsprung bicycle gears. Light planes, with only three wheels, are equally well represented by the small perturbation analysis. However, small perturbation applications to heavy transports are considered to be approximations, best at the low airspeed end of the rollout.

A complete six-degrees-of-freedom analysis is used to verify the accuracy of the small-perturbation analysis for the sailplane case. The complete equations are also used for the replication of Weick's historic rollout stability demonstration.

Tire Force and Moment Data

The equations of aircraft motion are usable in the study of directional stability during rollout, if one adds the external forces and moments transmitted from the ground to the tires. These forces and moments bear a similarity to the aerodynamic forces and moments acting on an unyawed wing at angles of attack. Figure 1 shows the analogy, using standard Society of Automotive Engineers tire definitions.[3] α in the tire case is the lateral slip angle, rather than angle of attack.

As in the aeronautical case, tire forces and moments can be reduced to dimensionless form. Dimensionless force and moment parameters are of most utility when the parameters apply over wide ranges of design variables. For wings, a particular lift coefficient gives the wing lift for geometrically similar wings of any area, air density, and flight velocity, provided that Mach and Reynolds numbers are not too different.

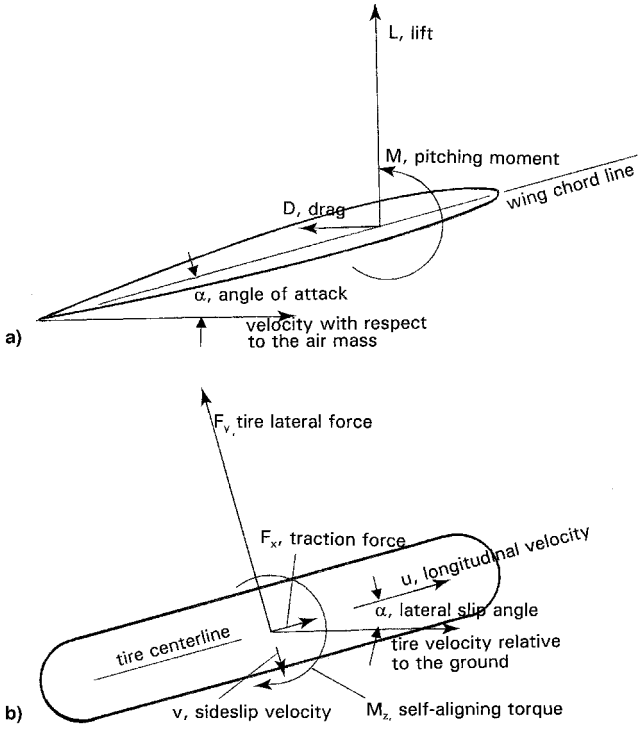

Fig. 1 Forces and moments acting on wings and tires: a) wing section and b) tire, top view.

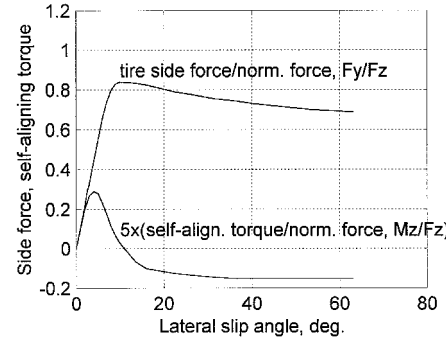

Fig. 2 Representative tire side force[5] and self-aligning torque[6] data.

Dimensionless tire parameters, such as the ones derived by Radt and Milliken,[4] apply reasonably well over ranges of tire diameter, construction type (radial or biased ply), camber angle, slip ratio, inflation pressure, load, and surface friction coefficient. However, for the limited purposes of this paper, we use tire data based on a simpler formulation.[5]

In the simpler model, tire traction and lateral forces F_x and F_y, respectively, are normalized by dividing by the tire normal load F_z. The yawing moment M_z, a self-aligning torque for small lateral slip angles α, is also divided by F_z, giving it the dimensions of length. Zero longitudinal slip ratio S is assumed. Zero slip ratio is appropriate to the landing rollout application, up to the moment that brakes are applied. Slip ratio is negative for traction, when power is applied to the wheels, and positive for braking.

Numerical data on F_x/F_z, F_y/F_z, and M_z/F_z are available from a number of sources.[5–7] These data are based on measurements on specific tires rotating against moving belts. Figure 2 provides representative examples of tire force and moment data. Except for the transient analyses of this paper, tire data are linearized, assuming small lateral slip, camber, and tire-steering angles. In the analysis that follows, shorthand symbols are assigned to the dimensionless traction force and to the derivatives with respect to lateral slip and camber angles of tire force and moment, as follows:

$$\mu = -\frac{F_x}{F_z}, \qquad y_\alpha = \frac{\partial(F_y/F_z)}{\partial \propto}$$
$$y_\gamma = \frac{\partial(F_y/F_z)}{\partial \gamma}, \qquad n_\alpha = -\frac{\partial(M_z/F_z)}{\partial \propto} \tag{1}$$

Tire Forces and Moments Applied to Airframe

Figure 3 is a plan view of a single tire relative to aircraft X- and Y-body axes. From the figure

$$u = U\cos PS + V\sin PS + SQ \times R\sin(PS - \tau)$$
$$v = -U\sin PS + V\cos PS + SQ \times R\cos(PS - \tau) \tag{2}$$

u and v are tire velocities relative to the ground, and U and V are aircraft velocity components on X and Z body axes. By the usual approximations in small-perturbation aircraft dynamics

$$U = U_0 + \mathrm{d}U, \qquad V = V_0 + \mathrm{d}V = \mathrm{d}V, \qquad R = R_0 + r = r$$

The steering angle PS is taken as a small angle. With these conditions, Eqs. (2) reduce to

$$u = U_0 + \mathrm{d}U - SQr\sin\tau, \qquad v = -U_0 PS + \mathrm{d}V + SQr\cos\tau \tag{3}$$

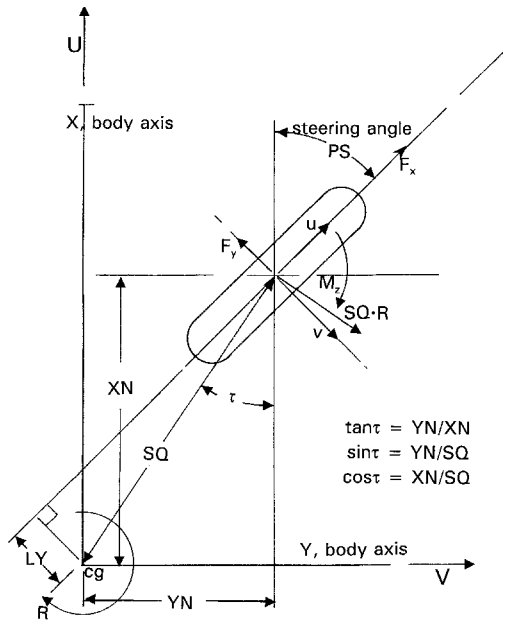

Fig. 3 Plan view of single tire, symbols, and definitions.

With $U_0 \gg dU - SQr\sin\tau$ and with the small-perturbation sideslip angle defined as $\beta = dV/U_0$, the tire lateral slip angle α reduces to

$$\alpha = v/u = \beta + rXN/U_0 - PS \tag{4}$$

From Eqs. (1)

$$F_x = -\mu F_z, \qquad F_y = y_\alpha F_z\alpha + y_\gamma F_z\gamma, \qquad M_z = -n_\alpha F_z\alpha$$

In this simplified analysis, tire and strut masses are lumped with the mass of the rest of the airframe. Thus, the tire vertical load F_z is the negative of the Z-body axis force acting on the airframe. Also, from Fig. 3

$$LY = SQ\sin(PS - \tau)$$

which by the small perturbation assumptions reduces to

$$LY = PS \times XN - YN$$

Finally, aircraft bank angle adds linearly to tire camber angle, so that perturbation camber, or γ, can be replaced by perturbation bank angle, or φ. The previous results lead to the following expressions for the perturbation (first-order) side force and yawing moment applied by the tires to the airframe:

$$\begin{aligned}\Delta Y &= -F_y\cos PS + F_x\sin PS \\ &= -y_\alpha F_z(\beta + XNr/U_0 - PS) - y_\gamma F_z\varphi - \mu F_z PS \\ \Delta N &= F_x LY - F_y(XN + PS \times YN) + M_z \\ &= -\mu F_z(PS \times XN - YN) - Y_\alpha F_z XN(\beta + rXN/U_0 \\ &\quad - PS) - y_\gamma F_z XN\varphi - n_\alpha F_z(\beta + rXN/U_0 - PS)\end{aligned} \tag{5}$$

Tire Stability Derivatives, Noncastering, Nonsteering Cases

Tires that are fixed in yaw, i.e., noncastering or nonsteering, are typical of main landing gears. Their contributions to rollout directional stability are found by extracting their stability derivatives from the general force and moment Eqs. (5). The noncastering, nonsteering case corresponds to zero values of the steering angle PS.

Taking derivatives of tire force and moment with respect to β and r leads to the following results for the stability derivative contributions of noncastering wheels:

$$\Delta Y_v \equiv \frac{(\partial Y/\partial\beta)}{U_0 m} = -\frac{y_\alpha F_z}{mU_0}, \qquad \Delta Y_r \equiv \frac{(\partial Y/\partial r)}{m} = -\frac{y_\alpha F_z XN}{mU_0}$$

$$\Delta N_v \equiv \frac{(\partial N/\partial\beta)}{U_0 I_z} = -\frac{(y_\alpha XN + n_\alpha)F_z}{U_0 I_z} \tag{6}$$

$$\Delta N_r \equiv \frac{(\partial N/\partial r)}{I_z} = -\frac{(y_\alpha XN + n_\alpha)F_z XN}{U_0 I_z}$$

Note that the lateral wheel location YN does not appear in Eqs. (6). The absence of the dimension YN means that rollout directional stability is the same for multiple tires as that for a single tire at the same longitudinal location. That is, the linearized equations cannot distinguish between bicycle gears and normal left and right gear pairs at the same fuselage station. Derivatives with respect to bank angle (equivalent to camber in this case) are not needed because the rollout perturbation stability analysis that follows is limited to two degrees of freedom, sideslip, and yawing velocity.

Tire Stability and Control Derivatives, Castering and Steering Cases

An equilibrium castering angle PS is found from the condition of zero tire sideslip velocity relative to the ground v and lateral slip angle α. Equilibrium in this context means that high-frequency castering rotations have died away after changes in tire velocities relative to the ground. Most castering gears have either friction or hydraulic dampers that produce this type of equilibrium in times that are short relative to aircraft responses.

For small wheel angles relative to the X-body axis and with the usual small perturbation approximations for aircraft motion variables, the $v = 0$ condition applied to the second of Eqs. (3) yields the castering wheel angle as

$$PS_{\text{castering}} = \beta + XNr/U_0 \tag{7}$$

Because the lateral slip angle α is taken as zero, so are M_z and n_α. Applying the castering condition Eq. (7) to the force and moment Eqs. (5), and taking derivatives with respect to β and r, leads to the following results for the stability derivative contributions of castering wheels, in their equilibrium state:

$$\Delta Y_v \equiv \frac{(\partial Y/\partial\beta)}{U_0 m} = -\frac{\mu F_z}{mU_0}, \qquad \Delta Y_r \equiv \frac{(\partial Y/\partial r)}{m} = -\frac{\mu F_z XN}{mU_0}$$

$$\Delta N_v \equiv \frac{(\partial N/\partial\beta)}{U_0 I_z} = -\frac{\mu F_z XN}{U_0 I_z} \tag{8}$$

$$\Delta N_r \equiv \frac{(\partial N/\partial r)}{I_z} = -\frac{\mu F_z XN^2}{U_0 I_z}$$

Comparing the castering derivatives in Eqs. (8) with the noncastering derivatives in Eqs. (6), the side force slope parameter y_α is replaced by the traction (in this case, friction) parameter μ. Also, terms involving the self-aligning torque parameter n_α are absent. μ is about two orders of magnitude smaller than y_α, as is n_α. The interesting conclusion is that the rollout directional stability contributions of castering nose or tail wheels are quite negligible compared with those of fixed wheels.

Tire control derivatives give a measure of linearized steering power and are needed for tire-implemented stability augmentation studies. These are derived from the force and moment equations [Eqs. (5)] by taking derivatives of tire force and moment with respect to steering angle PS:

$$\Delta Y_\delta \equiv \frac{(\partial Y/\partial PS)}{m} = -\frac{(\mu - y_\alpha)F_z}{m}$$

$$\Delta N_\delta \equiv \frac{(\partial N/\partial PS)}{I_z} = -\frac{(\mu - y_\alpha)F_z XN}{I_z} + \frac{n_\alpha F_z}{I_z} \tag{9}$$

Replication of Weick 1935 Demonstration

The 1935 demonstration by Weick of the rollout directional stability advantages of tricycle, or castering nose wheel landing gears, is replicated with a standard six-degrees-of-freedom aircraft transient response analysis program,[10] when tire force and moments are added to the equations of motion. Tire side force is represented by the linearized parameter y_α, with the force truncated at a tire slip angle α of 10 deg. The demonstration model, a triangular framework, is shown in Fig. 4.

Geometric model parameters are given in the figure. The vertical forces $ZLG(K)$ correspond to the static equilibrium condition, and are the negatives of the tire vertical load. Additional simulation parameters are $y_\alpha = 7.20$ (truncated at 10-deg slip angle), $\mu = 0.10$, m = 0.3106 (10 lb), $n_\alpha = 0.0$, $\omega = 10.0$, $\zeta = 0.30$, and $I_z = 0.0776$.

In the simulations, the model is launched at a heading or sideslip angle of 10 deg to the direction of motion, at a speed of 20 fps. Figure 5 gives the time histories of the subsequent nose wheel and heading angles for the tricycle gear case, in which the model is launched point forward. Heading angle damps to zero in less than 2 s. The model rolls straight ahead, stably.

Tail wheel and heading angles for the tail wheel case are shown in Fig. 6, after a launch with the model's point aft. The castering tail wheel quickly goes to its negative limit of 30 deg. The model diverges to the right from its 10-deg right yaw launching attitude, and executes a complete 180-deg ground loop in less than 1 s. This

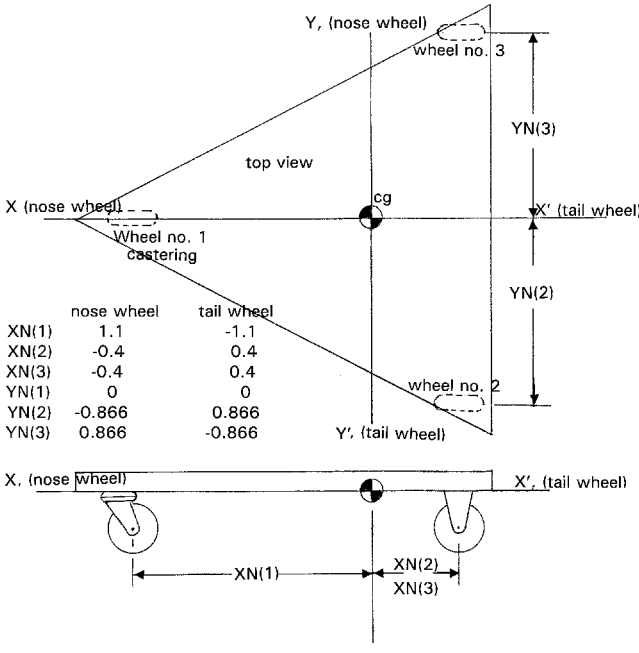

Fig. 4 Dimensions for computer replication of the 1935 Weick demonstration.

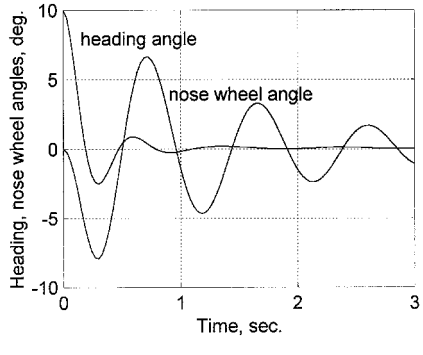

Fig. 5 Time history of replicated demonstration run, nose wheel landing gear.

Table 1 Parameters used in the linearized analysis

Parameter	SGS 1-34	Cessna 182	Boeing 747-100
b_w	49.17	35.8	195.68
C_L	0.18	0.46	0.90
$C_{n\beta}$	0.055	0.06455	0.184
C_{nr}	−0.074	−0.05924	−0.360
$C_{y\beta}$	−0.40	−0.3086	−1.08
C_{yr}	0.24	0.2103	0.300
I_z	2600	1967	45.4×10^6
m	26.0	90.14	17,515
S_w	151.08	164	5500
XN (nose)	——	——[a]	76.8
XN (main)	−0.49[b]	−1.3[b]	−5.3
y_α	7.2	7.2	7.2

[a]Castering nose wheel, not used in the calculation.
[b]Design value, varied in the calculations.

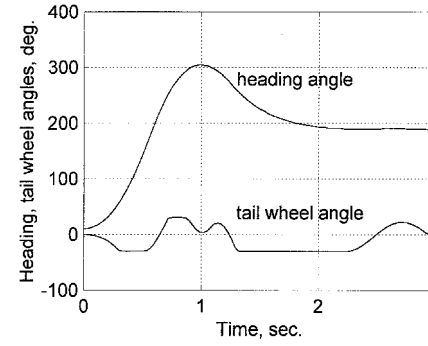

Fig. 6 Time history of replicated demonstration run, tail wheel landing gear.

puts it into the tricycle gear configuration, and it damps to a stable heading, rolling backward.

Effect of Landing Gear Location on Rollout Roots, Sailplanes, and Light Planes

While the Weick demonstration gives convincing proof of the landing rollout directional instability of tail wheel gear arrangements and the stability of tricycle, or nose wheel arrangements, it is instructive to examine the effect of gear location for actual aircraft configurations. Two example cases are chosen, the Schweitzer 1-34 standard-class sailplane, and the widely used Cessna 182 four-place light plane.

The sailplane case is of special interest because there is a strong incentive for designers to use the equivalent of a tail wheel-type landing gear, with the main gear, a single wheel, located ahead of the c.g. This arrangement avoids the need for a nose skid or wheel, and makes it easier to get a low drag forward fuselage shape. A tail wheel used in such an arrangement is generally noncastering, but it does not provide stability until it carries weight, which is at very low airspeeds.

Rollout eigenvalues or roots are found for a two-degrees-of-freedom linearized model, with sideslip and yaw rate variables. The noncastering wheel stability derivative contributions [Eqs. (6)] are used. Elements of the LOCUS program of Ref. 10 are used to calculate eigenvalues for the system defined by the state matrix equation $\dot{x} = Ax$, where

$$x = \{v \quad r\}, \qquad A = \begin{bmatrix} Y_v + \Delta Y_v & Y_r + \Delta Y_r - U_0 \\ N_v + \Delta N_v & N_r + \Delta N_r \end{bmatrix}$$

The symbols preceded by deltas are the noncastering derivative contributions of Eq. (6). Numerical values for the parameters used in the calculations are given in Table 1.

The rollout stability eigenvalues for the Schweitzer 1-34 are shown in Fig. 7, as a function of fore and aft main gear location

XN. The ground speed is 40 fps. There are two real roots. Divergence is predicted not for all wheel positions forward of the c.g., but only when the wheel is more than 0.7 ft ahead. The tire contributions dominate the aerodynamic terms at 40 fps.

Stability results for the Cessna 182 are shown in Fig. 8, at three rollout speeds. The nose wheel is assumed to be unloaded in these calculations. Eigenvalues are stable complex conjugates at 40 and 60 fps, for aft main gear locations. As with the previous sailplane example, one real unstable root emerges when the main gear location is slightly ahead of the c.g.

Rollout Roots, Large Airplanes with Noncastering Nose Wheels

Large airplanes, such as jet transports, require nose wheel power steering. Their nose wheels are noncastering,[7,8] except for ground handling under tow. The noncastering tire stability derivative contributions of Eqs. (6) apply to all wheels during landing rollout.

A simple result is obtained for the directional stability derivative ΔN_v for the noncastering case where tire loads are distributed between nose and main gears inversely to their respective lever arms. This condition, called "balanced wheel loads" in this paper, is of course the situation when the airplane is at rest on the ground. The following analysis supposes that the balanced wheel load distribution occurs during rollout as a result of the pilot's use of longitudinal control. With index $K = 1$ for the nose wheel and $K = 2$ for the lumped main wheel reactions, the balanced wheel load condition is

$$ZLG(1)XN(1) + ZLG(2)XN(2) = 0 \tag{10}$$

Using Eq. (10) in Eq. (6), assuming the same values of the dimensionless tire force parameter y_α, and neglecting the small tire alignment torque term n_α, the tire contribution to static directional stability ΔN_v vanishes.

The tires still contribute to yaw damping through ΔN_r, and the overall small-perturbation motion is stable, just as for the classical tricycle gear with castering nose wheel. This is shown in Fig. 9, which presents rollout roots for the Boeing 747-100 airplane, as a function of airspeed. Numerical values for the calculations are given in the last column of Table 1, based on Ref. 9, for the maximum gross weight landing configuration. The balanced wheel load distribution of Eq. (10) applies.

For comparison, Boeing 747-100 rollout roots are also shown for the loading shifted aft entirely to the main wheels. Aft wheel loadings would occur as a result of landing spoiler deployments or aft

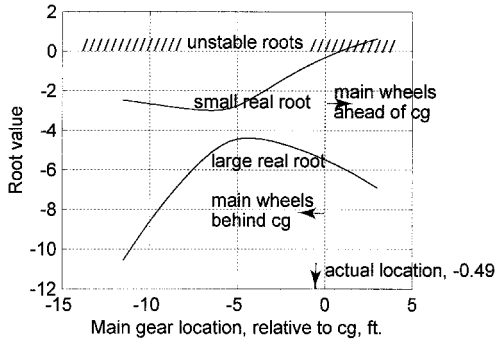

Fig. 7 Effect of main gear location on lateral roots in rollout, Schweitzer 1-34 at 40 fps.

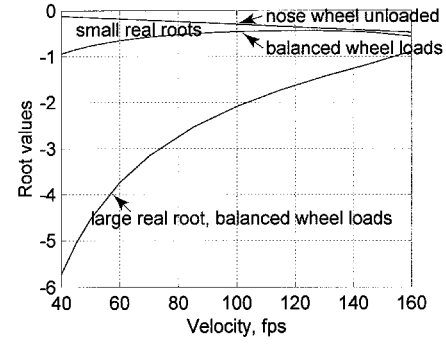

Fig. 9 Effect of airspeed on lateral roots in rollout, Boeing 747-100. Large real root for nose wheel unloaded case off scale negatively.

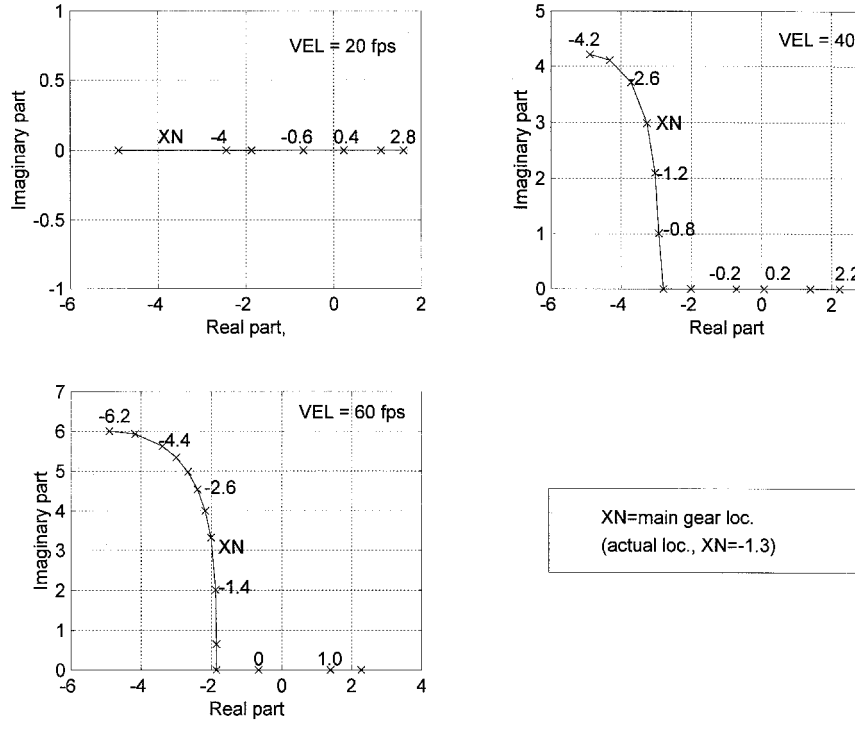

Fig. 8 Effect of main gear location on lateral roots in rollout, Cessna 182 at 20, 40, and 60 fps. Roots within circle not shown.

control column positions. The large real root is increased negatively off scale in Fig. 9, while the small real root is only slightly changed. The conclusion is that aft loadings are somewhat stabilizing in rollout for noncastering nose gear configurations.

Locked Tail Wheels and Tail Skids

The previous results for noncastering nose wheels with balanced wheel loads apply as well to tail wheel airplanes with locked tail wheels. That is, the tire contribution to static directional stability is zero. Tail wheels must caster for maneuvering around airports at taxi speeds of a few knots, but directional instability during landing rollout and takeoff roll is avoided if the tail wheel can be locked and is bearing weight at least in proportion to its moment arm to the c.g. Because the tail wheel is not usually loaded at the higher ground speeds, lockable tail wheels are not a complete solution to the directional stability problem. From the stability standpoint, tail skids are equivalent to locked tail wheels.

Transient Response Results, Sailplane (Bicycle Gear) Case

Transient response calculations[10] are made for the Schweitzer 1-34 sailplane for the actual main wheel location of 0.49 ft behind the c.g., and assumed locations of 0.49, 1.00, and 1.50 ft ahead of the c.g. The latter cases represent the class of sailplanes in which ground handling stability is compromised to get rid of drag producing devices such as the 1-34's forward skid. A small noncastering tail wheel is located 16 ft behind the c.g., making the arrangement a bicycle gear. However, these calculations consider only main wheel forces, applying to the portion of the landing rollout that is made at near level attitudes, with nose or tail skids or wheels not hitting the ground.

The simulations start just after touchdown, at an airspeed of 70 fps, or 41 kn. Aileron and elevator feedback loops are closed, representing a pilot's assumed activities in holding the wings level and keeping a reasonable pitch attitude. The runs are made with neutral rudder angles, as a check on the eigenvalues previously found. A 10 fps side wind doublet at the start of the ground roll serves to excite lateral motions.

Figure 10 shows the effects of main gear position on heading angle. Rollout is stable for the two rearmost gear locations, but progressively divergent with more forward gear locations, agreeing with the linearized analysis. Additional runs, not shown, verify that closing the rudder loop to the runway centerline, as would be done by a pilot, prevents divergence for all gear locations, up to the point of full rudder deflection.

Bank into Swerve Strategy

As airspeed bleeds off during landing rollouts, sailplanes or other airplanes with bicycle or tandem landing wheels cannot maintain straight courses in the face of side winds. At some low airspeed, the rudder goes to its stop, or saturates, in countering the yawing moment caused by static directional stability N_v. A swerve starts into the relative wind. This is true regardless of whether the main

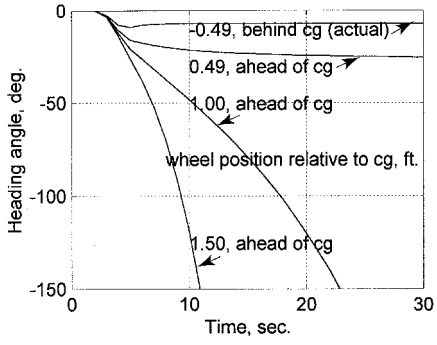

Fig. 10 Effect of main gear location on directional stability of Schweitzer 1-34 sailplane, rudder locked, roll and pitch atitudes controlled to zero, lateral gust doublet from 1 to 5 s.

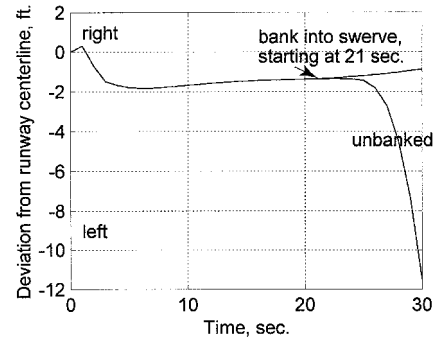

Fig. 11 Bank into swerve strategy; Schweitzer 1-34 with main gear ahead of c.g. Left bank into left crosswind when rudder saturates to the right and aircraft starts left swerve at 21 s.

wheel is ahead of or behind the c.g., although simulation shows an earlier rudder control saturation in the former case.

With the common high-performance sailplane configuration of a main wheel ahead of the c.g., straight ground courses can be maintained after rudder control saturation by the counter-intuitive strategy of banking into the swerve direction, or into the relative wind. This is illustrated in Fig. 11. When a 10-deg left bank into the left swerve is started at 21 s, divergence is avoided.

The corrective moment is the yawing moment about the main gear of the wing lift component parallel to the ground. With aft main gear locations, banking away from the swerve maintains straight ground tracks in crosswinds. Allowable bank angle is limited by ground clearance, and is as low as 7 deg for some sailplanes.

Conclusions

1) Lateral-directional stability derivative contributions for aircraft tires can be developed for both castering and noncastering wheels. These derivatives can be added to conventional aircraft stability derivatives to treat cases of aircraft in ground rolls.

2) Tire yawing moment and side force derivatives for castering wheels are negligible as compared with those for noncastering wheels.

3) Tire yawing moment and side force control derivatives can be derived for studies of stability augmentation systems implemented by wheel steering rather than control surface deflection.

4) For the linearized analysis, rollout directional stability and control are the same for single tires as for multiple tires at the same longitudinal (fuselage) station. Tire spanwise location is also not a factor.

5) For both sailplane (bicycle) and light plane (three-wheel) cases, linearized analysis predicts directional divergence for main gears slightly ahead of the c.g.

6) Within the limitations of the linearized analysis, the Boeing 747-100, typical of large airplanes with noncastering nose wheels, is directionally stable over the landing rollout airspeed range, for a range of relative loadings of main and nose gears. This class of stability occurs also for tail wheel airplanes with locked tail wheels that are carrying load.

7) Nonlinear transient response analysis confirms linearized eigenvalue analysis results on the effect of main gear location relative to the c.g., for the sailplane example of this paper.

8) For bicycle gears, or advanced sailplanes having forward main gear locations, a bank into swerve strategy for avoiding running off runways in side winds, after the rudder reaches its stops, is validated in simulation. The lateral component of the tilted lift vector provides the necessary yawing moment about the main gear contact point.

References

[1] Weick, F. C., and Hansen, J. R., *From the Ground Up*, 1st ed., Smithsonian Institution Press, Washington, DC, 1988, pp. 131–149.

[2] Weick, F. C., "Everyman's Airplane—A Move Toward Simpler Flying," *S.A.E. Journal (Transactions)*, Vol. 38, No. 5, 1936, pp. 176–189.

[3]"Vehicle Dynamics Terminology," Society of Automotive Engineers, Rept. J670e, Warrandale, PA, June 1978.

[4]Radt, H. S., Jr., and Milliken, W. F., Jr., "Non-Dimensionalizing Tyre Data Vehicle Simulation," *Road Vehicle Handling*, Inst. of Mechanical Engineers, Conference Publications 1983-5, 1983, London, pp. 229–240.

[5]Allen, R. W., Magdaleno, R. E., Rosenthal, T. J., Klyde, D. H., and Hogue, J. R., "Tire Modeling Requirements for Vehicle Dynamics Simulation," *S.A.E. Transactions*, Vol. 104, Sec. 6, 1995, pp. 484–506.

[6]Bakker, E., Nyborg, L., and Pacejka, H. B., "Tyre Modelling for Use in Vehicle Dynamics Studies," *S.A.E. Transactions*, Vol. 96, Sec. 2, 1987, pp. 190–204.

[7]Currey, N. S., *Aircraft Landing Gear Design: Principles and Practices*, 1st ed., AIAA, Washington, DC, 1988, pp. 132, 133.

[8]Young, D. W. S., and Ohly, B., "European Aircraft Steering Systems," *Aerospace Technology Conference and Exposition*, Society of Automotive Engineers, Publication PT-37, Warrandale, PA, 1985, pp. 112–130.

[9]Heffley, R. K., and Jewell, W. F., "Aircraft Handling Qualities Data," NASA CR-2144, Dec. 1972.

[10]Abzug, M. J., *Computational Flight Dynamics*, 1st ed., AIAA, Reston, VA, 1998, pp. 99–130, 151–196.